

# Flux-pinning mechanism of proximity-coupled planar defects in conventional superconductors: Evidence that magnetic pinning is the dominant pinning mechanism in niobium-titanium alloy

L. D. Cooley

*Electromagnetic Technology Division, National Institute of Standards and Technology, 325 Broadway, Boulder, Colorado 80303*

P. J. Lee and D. C. Larbalestier\*

*Applied Superconductivity Center, University of Wisconsin-Madison, 1500 Johnson Drive, Madison, Wisconsin 53706*

(Received 29 June 1995; revised manuscript received 14 November 1995)

We propose that a magnetic pinning mechanism is the dominant flux-pinning mechanism of proximity-coupled, planar defects when the field is parallel to the defect. We find compelling evidence that this pinning mechanism is responsible for the strong flux-pinning force exerted by ribbon-shaped  $\alpha$ -Ti precipitates and artificial pins in Nb-Ti superconductors, instead of the core pinning mechanism as has been hitherto widely believed. Because the elementary pinning force  $f_p(H)$  is *nonmonotonic* when it is optimum (i.e., when the defect thickness  $t$  and the proximity length  $\xi_N$  have comparable dimensions), the total pinning force  $F_p(H)$  generally does *not* show temperature scaling. Characteristic changes in the magnitude and shape of  $F_p(H)$  at constant  $T$  but at different  $t/\xi_N$  (e.g., different Nb-Ti wire diameters) are also direct consequences of the pinning mechanism. The optimum flux-pinning state is a compromise between maximizing  $f_p$  and getting the highest number density of pins. For a given defect composition this state is reached when  $t \sim \xi_N/3$ , while for varying defect composition the peak  $F_p$  gets higher when  $\xi_N$  is made shorter. Artificial pinning center Nb-Ti wires having short  $\xi_N$  pins appear to be vital for obtaining high  $J_c$  at high fields because only then is the elementary pinning force optimized at small pin thicknesses which permit a high number density of vortex-pin interactions and a large bulk pinning force. We find verification of our predictions in experimental  $F_p(H, T, t)$  data obtained on special laboratory-scale artificial pinning-center Nb-Ti wires.

## I. INTRODUCTION

Strong flux-pinning forces and high critical current densities  $J_c$  are readily obtained by filling a superconductor with a high number density of thin planar defects.<sup>1,2</sup> The constraints on making such superconductors usually cause the defects to become strongly coupled to the matrix by the proximity effect.<sup>3</sup> Thus, it immediately becomes difficult to determine how to optimize (i.e., obtain maximum  $J_c$ ) a given flux-pinning system because the dominant flux-pinning mechanism(s) must be evaluated in the context of the superconducting order parameter variations caused by the proximity effect. As a result, the influence of important materials properties may be misinterpreted.

This problem is demonstrated in thermomechanically processed (TMP) niobium-titanium alloy (chiefly Nb 47 wt.% Ti or Nb47Ti). The empirical processes by which a TMP Nb-Ti superconductor may be optimized are based on fluxon core-pinning models.<sup>4-8</sup> Continuous deformation of the microstructure prior to optimization is thought to cause competition between several flux pinning mechanisms, including core pinning, as the number densities of various microstructural defects change.<sup>5-12</sup> At optimum wire diameter, microstructures contain about 20% of 1–4 nm thick, ribbon-shaped  $\alpha$ -Ti precipitates which are separated by 2–10 nm.<sup>7,13</sup> Both dimensions are smaller than the diameter (11 nm) and spacing (22 nm) of the fluxon cores at 5 T, 4.2 K.<sup>8</sup> Although the precipitates seem to be too thin to strongly interact with the fluxon core,<sup>8,14</sup> other data are in agreement with core

pinning being the dominant pinning mechanism: The precipitate number density far exceeds the number density of all other defects,<sup>7</sup> the functional dependence of the derived elementary pinning force  $f_p$  appears to be consistent with core pinning models,<sup>8</sup> and the shape of the bulk pinning force curve  $F_p(H) = \mu_0 J_c(H)$  is proportional to  $h(1-h)$ ,<sup>5,8</sup> where  $h \equiv H/H_{c2}$ ,  $H$  is the external field strength, and  $H_{c2}$  is the upper critical field.

Core-pinning models give the enticing prediction that new artificial pinning center (APC) wires can dramatically improve superconducting wire performance because they can incorporate number densities of pins that are higher and pin materials that are better than in TMP composites. However, the relationship between the microstructure and the flux-pinning properties of APC composites is not the same, as we will describe in this paper. A central difficulty is that, although the available transmission electron microscopy (TEM) data<sup>15-17</sup> show that the optimum pin thickness seems to be *better* suited for core pinning in optimized APC composites with Nb pins, the  $F_p$  curves do *not* show the characteristic  $h(1-h)$  shape expected for core pinning. Instead,  $F_p(h)$  typically has a peak at  $h \sim 0.25$ , as shown in Fig. 1. (APC wires with pins other than Nb have only very recently been made; data that are representative of the intrinsic flux-pinning properties of their microstructure have yet to be published.) The relative lack of high-field pinning is the primary reason why the enormous potential of APC designs has not yet been realized in high-field applications.

This paper aims to resolve the surprisingly different flux-

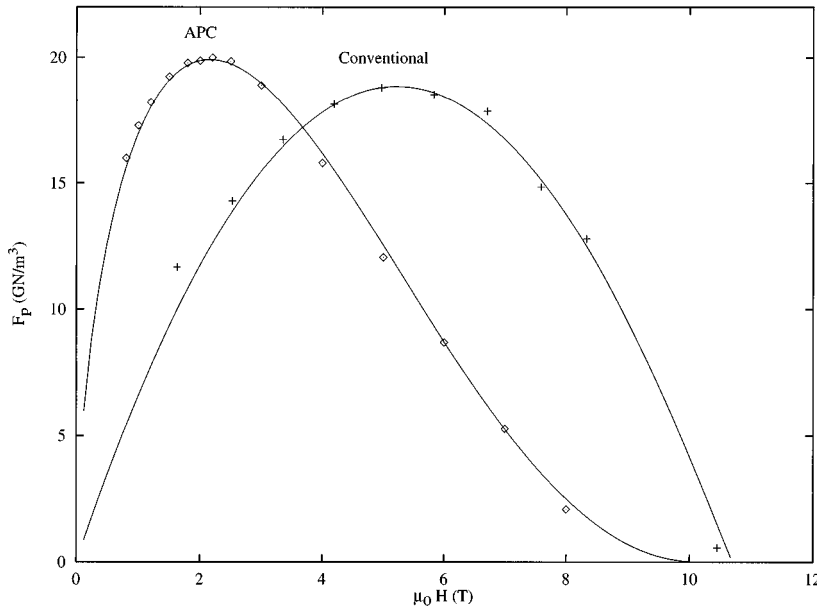


FIG. 1. Comparison of optimized bulk pinning force curves for conventional and APC wires. The data for the conventional wire were obtained from Ref. 8 and the data for the APC wire from this paper.

pinning behavior of TMP and APC designs by reinterpreting their dominant pinning mechanisms in the context of the proximity effect. We propose that *magnetic* pinning is the dominant pinning mechanism in both composite types, instead of core pinning. Further, since the arguments made in this paper are based on general phenomena that occur in all superconductors, the conclusions may be applied to the flux-pinning properties of any superconductor that contains thin, proximity-coupled, planar pins as the dominant microstructural defect.

Although other flux-pinning models<sup>18,19</sup> give reasons why  $F_p(H)$  might change shape when the pin composition is changed and/or when the microstructural dimensions are changed, we frame our model within phenomenological arguments that can be or have been tested experimentally. We pay particular attention to the Nb-Ti system, which has been extensively studied. In particular, the electron scattering mechanism<sup>18</sup> provides a detailed quasiclassical analysis for determining the pinning energy as a function of the concentration and electron scattering cross section of the pin, but it cannot be used for evaluating the pinning energy arising from the order-parameter variations due to the proximity effect. We think the details of the proximity coupling are crucial: In APC Nb-Ti composites,  $F_p(H)$  reaches very high values at low fields and has a long tail at high fields when artificial Nb pins are thick,<sup>17,21,22</sup> but takes on a mid-field peak and a shape characteristic of core pinning when the pins are very thin.<sup>23,24</sup> Nb pins become strongly proximity coupled when thin, as demonstrated by the reduction of  $H_{c2}$ .<sup>21,23,25,26</sup> By contrast, there is no shift of the peak of  $F_p(H)$  to higher fields in TMP wires when the wire is drawn past its optimum diameter.<sup>27,28</sup>

The basis of our arguments is the recent model of Gurevich and Cooley<sup>29</sup> for magnetic pinning by a planar contact, with elements of proximity-effect theory added. The proximity length  $\xi_N$  and the decoupling field  $H_d$  then become central parameters of our model. We find that there is always a strong magnetic interaction between a fluxon and a ribbon, because a portion of the shielding current (on the order of the depairing current density  $J_D$  next to the vortex core) cannot

be transmitted across the ribbon. These ideas have been briefly outlined in an earlier paper.<sup>30</sup> We will show that the different flux-pinning properties of Nb and  $\alpha$ -Ti result more from differences in their electronic properties than from differences between average pin thickness and the diameter of the fluxon core.

The elementary magnetic pinning force  $f_p$  increases slightly with field because the pin becomes less transparent to current as its proximity coupling decreases. Thus the magnetic component peaks at the decoupling field. This complicates summation: Although *thick* pins with a *long* proximity length can have the same  $f_p$  value as *thin* pins with a *short* proximity length, the *bulk* pinning force  $F_p \approx n f_p$  is maximum for pins with *short* proximity length, because thin pins produce a higher number density of pinning interactions  $n$  for a given pin volume fraction. Additionally, the combination of the nonmonotonic field dependence of the elementary pinning force with changes in temperature or pin thickness gives rise to other unusual properties of the bulk pinning force, such as a lack of temperature scaling. We take advantage of experimental observations of such phenomena to fully test the model.

We analyze experimentally the bulk pinning force of a multifilament Nb47Ti APC composite having Nb 1.3 wt.% Ti (Nb1Ti) pins. By careful processing under laboratory conditions, we produced a pin array which was uniform down to  $\sim 30$  nm pin separation.<sup>15</sup> We have extended the microstructural characterization<sup>15</sup> to pin thicknesses approaching 1 nm, much less than the coherence length. We directly observe the transition of the pin cross section from a round to a ribbon shape. Further, we observe that the pin thickness distribution is more narrow than that of  $\alpha$ -Ti precipitates in a conventional composite. We used newly developed techniques<sup>31</sup> to estimate the pin thickness from the TEM observations, and we were then able to make a quantitative comparison between our magnetic pinning model and the TEM data.

We made flux-pinning measurements over the full range of field, temperature  $T$ , and pin thickness  $t$  in order to explore the effect of  $\xi_N(T)$  and the coherence length  $\xi(T)$  on the flux-pinning parameters. We observed (1) a lack of tem-

perature scaling of  $F_p(H)$  for any given pin thickness [temperature scaling requires that  $F_p(H)$  has a constant shape independent of temperature<sup>32</sup>]; and (2) a systematic variation of  $F_p(H)$  as a function of  $t$ . A lack of temperature scaling and a variation of  $F_p(H)$  with changing precipitate thickness was reported earlier for conventional Nb47Ti,<sup>8</sup> as well as for conventionally processed alloys having compositions ranging from Nb 44 wt.% Ti to Nb 62 wt % Ti.<sup>33</sup>

There is excellent qualitative agreement between experimental data and the model. We predict that  $F_p$  reaches a maximum when  $t \approx \xi_N/3$ . Pins like  $\alpha$ -Ti, which have small  $\xi_N$ , produce maximum  $F_p$  when the pins are thin and have high number density, thus providing  $F_p(H)$  curves which peak at fields near  $0.5H_{c2}$ . By contrast, pins with larger  $\xi_N$ , like Nb and Nb1Ti, are thicker and have a lower number density when optimized, so the peak of  $F_p(H)$  occurs at lower fields. Thus, intelligent pin design is crucial to attaining high critical current density at higher fields where it is most desirable. Not only is it necessary to prevent  $H_{c2}$  depression by choosing the correct matrix and pin composition; it is also vital to alloy the pin material to reduce the electron mean free path and  $\xi_N$  so that the elementary pinning force is optimum at pin thicknesses less than 5 nm, where corresponding pin number densities are comparable to high-field fluxon number densities. Thus, the crucial difference between APC composites made with Nb pins and conventional composites made with  $\alpha$ -Ti precipitates is that  $\alpha$ -Ti precipitates are naturally alloyed with  $\sim 5$  wt % Nb and thus have a smaller proximity length.

## II. FLUX-PINNING MODEL

### A. Pinning by planar defects with zero thickness

Consider an Abrikosov (A) vortex in a Cartesian coordinate system aligned parallel to  $z$  and lying near a  $yz$  plane. The vortex lies on the  $x$  axis at coordinate  $s$ ; the plane intersects  $x=0$ . The flux pinning potential  $U$  of this pinning plane is determined by the free energy difference (per unit length) between when the vortex is isolated within the superconducting matrix and when the vortex intersects the plane. An isolated vortex located at  $s > \lambda$  is unaffected by the plane and has an energy per unit length

$$U_A = \epsilon_0(\ln \kappa + \gamma_A), \quad (1)$$

where  $\epsilon_0 = 0.5\mu_0 H_c^2 \pi \xi^2$  is the line tension of the vortex, the logarithmic term represents the kinetic energy of the currents around the vortex core, and the constant  $\gamma_A = 0.5$  provides a small correction for the core (0.12) and the contribution of currents within the core itself (0.38).<sup>34</sup> In contrast, when the vortex is located at  $s < \lambda$ , the shielding current may be blocked or diverted by the plane, giving rise to magnetic pinning.<sup>4</sup> This is especially true for the ribbon-shaped pins found in both conventional and APC Nb-Ti wires.

Gurevich and Cooley<sup>29</sup> treated such a planar pin as a Josephson contact characterized by its transmission current density  $J_p$ . The magnetic pinning force is then described by the equations of Josephson electrodynamics. If the defect is weakly coupled to the superconducting matrix,  $J_p < J_D/\kappa$ , where  $J_D = 0.54H_c/\lambda$  is the depairing current density in the superconductor. The equations are *local*, and a Josephson ( $J$ )

fluxon exists when  $s=0$ .<sup>35</sup> The  $J$  fluxon has no core and is described only in terms of the phase of the superconducting order parameter on either side of the contact. In the opposite limit,  $J_D/\kappa < J_p < J_D$ , an analytic solution to the *nonlocal* equations<sup>36,37</sup> describes an intermediate vortex geometry for  $s=0$ , a so-called Abrikosov-Josephson or *AJ* vortex. The *AJ* vortex is similar to the usual *A* vortex in that it has nearly circular shielding currents and extends magnetically to a distance  $\sim \lambda$ . However, the *AJ* vortex is also similar to a *J* vortex in that it does not have a core. The solutions of the nonlocal Josephson electrodynamic equations that give the *AJ* vortex incorporate both the transmission of shielding current of magnitude  $J_p$  through the contact and the diversion of larger shielding current around the contact.

The current transmitted across the pin is the important parameter of this pinning mechanism; it divides flux pinning regimes. If  $J_p$  is very low, the current is diverted parallel to the defect as it is at a superconductor surface, and the *A* vortex is attracted to the contact by its antivortex image.<sup>38,39</sup> A strong pinning interaction results, where the pinning potential for  $\xi < s < \lambda$  is

$$U(s) = \epsilon_0[U_A - \ln(\lambda/s)]. \quad (2)$$

The elementary pinning force  $f_p(s) = -dU(s)/ds$  thus approaches its theoretical maximum<sup>4</sup> at  $s = \xi$ ,  $f_{\max} = -\epsilon_0/\xi$ , and then decreases like  $\lambda/s$  for  $s > \xi$ .

In the nonlocal limit, the pins are strongly coupled. The contact then is transparent to the shielding currents located at the outside edge of the *A* vortex, and no magnetic interaction occurs until the *A* vortex is within a distance  $l$ ,

$$l = \xi(J_D/J_p), \quad (3)$$

from the boundary. When  $s < l$  the contact perturbs the shielding current. The elementary pinning force is not as strong as in the local limit because the attraction of the *A* vortex to its antivortex image is offset by its repulsion from a second vortex image. The pinning potential is<sup>29</sup>

$$U(s) = \epsilon_0 \left( U_A + \ln \frac{s}{s+l} + \frac{l}{2s+l} \right). \quad (4)$$

The first term reflects the interaction between the vortex and its antivortex image, while the second term arises from the interaction between the vortex and its vortex image. The pinning potential has a width of order  $l$ , as opposed to the longer length  $\lambda$  in the local case. Its magnitude is of order  $\ln(l/\xi) + 0.22$ .<sup>40</sup> The maximum elementary pinning force again occurs at  $s = \xi$ , where

$$f_{\max} \approx -\frac{\epsilon_0}{\xi} \left[ \frac{l}{\xi+l} - \frac{2l\xi}{(2\xi+l)^2} \right]. \quad (5)$$

Thus,  $f_{\max}$  is slightly less in magnitude than  $\epsilon_0/\xi$ .

The pinning force is strong,  $\sim \epsilon_0/\xi$ , despite the very different behavior of vortices near the contact for different  $J_p$ . This is true because the shielding current near the vortex core, which is of order  $J_D$ , is perturbed, even for strongly coupled planar defects. The *A* vortex core *always* disappears at  $s \sim \xi$ . Thus, since  $J_p < J_D$  is practically true for any pin thickness, field, or temperature, there is no field or temperature at which the planar pin becomes ineffective. Also, be-

cause of the dependence of  $U$  on  $J_p$  given by Eqs. (3) and (4), the field and temperature dependence of  $f_{\max}$  incorporates that of  $J_p$ , and is not only controlled by the field and temperature dependence of the superconducting order parameter. Thus, it can no longer be assumed that  $f_{\max}(h) = f_{\max}(0)(1-h)$ , as is commonly believed for the core-pinning mechanism.<sup>4</sup> Instead, a lack of temperature and field scaling is built into this pinning mechanism.

### B. Pinning by planar defects with nonzero thickness: The role of the proximity effect

The microscopic mechanisms that determine  $J_p$  for a thin nonsuperconducting metal ( $N$ ) proximity coupled to a superconductor ( $S$ ) have been extensively studied.<sup>3,41-43</sup> We anticipate that dirty limit solutions are appropriate for the Nb1Ti pins used in our APC composite because Nb1Ti is itself a moderately dirty superconductor.<sup>32</sup> Also, the BCS coherence length  $\xi_0$  is about 40 nm for pure Nb and Nb-Ti alloys with  $\leq 65$  at.% Ti,<sup>44,45</sup> and with the dirty-limit Ginzburg-Landau expression  $\xi^2 = \phi_0/2\pi\mu_0 H_{c2} = 0.75\xi_0 l_{tr}$ , with  $\mu_0 H_{c2} \approx 1$  T at 4.2 K,<sup>32</sup> the mean free path  $l$  of Nb1Ti is 10.6 nm. This value is in excellent agreement with the resistivity data for Nb-Ti alloys obtained by Berlincourt and Hake.<sup>46</sup> The pin thickness observed by TEM ranges from  $\sim 3l$  to  $\sim 0.2l_{tr}$ , so the clean-limit condition  $l_{tr} \gg \hbar v_F/2\pi k_B T = \xi_0 T_c/T$  is not satisfied, where  $\hbar$  is the modified Planck constant,  $v_F$  is the Fermi velocity, and  $k_B$  is Boltzmann's constant.

The proximity effect is usually studied by using the Usadel equations.<sup>42</sup> These equations are valid when the critical temperature  $T_{cN}$  of the  $N$  layer is zero and the temperature is near  $T_c$ . They become linear when the  $N$  and  $S$  layer thicknesses are larger than  $\xi_N$ , where

$$\xi_N(T) = \left( \frac{\hbar v_F l_{tr}}{6\pi k_B T} \right)^{1/2}. \quad (6)$$

The proximity length is 11.9 nm at  $T_c$  and  $\xi_N/\xi \approx 3.3$  at 4.2 K for Nb1Ti pins in a Nb47Ti matrix. Thus, the conditions for the application of the linear Usadel equations should be satisfied when the field is higher than the upper critical field of the Nb1Ti pins and when the pin thickness is greater than 12 nm.

When the  $N$  layer is thin or when  $T_{cN}$  is comparable to  $T_c$ , the Usadel equations become dependent on the spatial variation of the superconducting order parameter in the  $N$  layer  $\Delta_N$ . In this limit we draw upon the work of Mota *et al.*,<sup>47</sup> who obtained an experimental determination of  $\Delta_N(x)$  by measuring the superheating and supercooling temperatures corresponding to the first-order phase transition of  $\Delta_N$  (see also Ref. 43). They used Nb and Nb-Ti proximity-coupled to Cu or Ag, and explored the regime  $t \ll \xi_N$  by measuring at temperatures of a few millikelvins. The gap as a function of position  $x > 0$ , for the  $N/S$  interface at  $x = 0$ , was found to obey the relation

$$\Delta_N(x) \propto \frac{x_0}{x + x_0} e^{-x/\xi_N} \quad (7)$$

when  $0.01\xi_N \leq t \leq 0.1\xi_N$ . This result was also obtained in an approximate solution to the Gor'kov equations by Falk<sup>48</sup> for

semi-infinite  $N/S$  regions in contact. The fitting parameter  $x_0$  should have a lower bound of  $\xi$ , since the order parameter should not change over smaller lengths. We take  $x_0 = 2\xi$ . Even though the Usadel equations should not be valid when  $t \ll \xi_N$ , Mota *et al.* found good qualitative agreement between their data and the theory. The proximity coupling of the pins exponentially decreased with field, with the decay constant given by the decoupling field,

$$H_d = H_{c2} \frac{x_0}{t + x_0} e^{-t/\xi_N}. \quad (8)$$

This expression has the correct asymptotic behavior:  $H_d \rightarrow H_{c2}$  as  $t \rightarrow 0$  and  $H_d \rightarrow 0$  when  $t \gg x_0$ . Measurements of the twist-pitch dependence of the magnetization for multifilament Nb-Ti/Cu composites which are in agreement with Eq. (8) have been obtained by Akune *et al.*<sup>49</sup>

Since we did not observe the anomalous behavior of  $H_{c2}(T)$  which is seen in multilayer Nb/Nb-Ti and Nb/Nb-Zr having equal Nb and Nb-alloy thicknesses,<sup>50,51</sup> we conclude that the nucleation of superconductivity always occurs within the Nb47Ti matrix,<sup>43,52</sup> even when both the pin and superconductor thicknesses are much less than  $\xi_N$ . Thus the results of Mota *et al.* for proximity-coupled Cu and Ag should also be valid for Nb1Ti, even when the applied field is below the upper critical field of the Nb1Ti pins and when the pin thickness and separation are less than  $\xi_N$ .

Within this framework, we apply the results of Mota *et al.* to the work of Dobrosavljević-Grujić and Radović,<sup>53</sup> who explicitly solved the Ginzburg-Landau equations for vortices lying within a thick  $SNS$  contact.  $J_p(H, T, t)$  then has an exponential dependence on  $t$  at zero field,

$$J_p(0, T, t) = J_0(T) e^{-t/\xi_N(T)}, \quad (9)$$

with

$$J_0(T) \approx J_D(0) \frac{2.6\xi(T)}{\xi_N(T)} (1 - T/T_c)^2. \quad (10)$$

$J_0$  is thus on the order of  $J_D$ ; however, it has a different temperature dependence,  $J_0(T) \propto [H_{c2}(T)]^2$ . When  $H \gg H_d$ , the pair condensation amplitude is diminished exponentially in the  $N$  layer, giving

$$J_p(H, T, t) = J_0(T) \frac{\xi_N(T)}{t} \frac{H_d}{H} e^{-H/H_d}. \quad (11)$$

To reflect the expectation<sup>53</sup> that  $J_p$  is not strongly field dependent for  $0 \leq H \leq H_d$ , we use a quadratic interpolation formula:

$$J_p(H, T, t) = J_0(T) \left[ e^{2t/\xi_N} + \left( \frac{2.6t}{\xi_N} \frac{H}{H_d} \right)^2 e^{2H/H_d} \right]^{-1/2}. \quad (12)$$

The exponential behavior of  $J_p$  at high field and the increase of  $J_p/J_0$  as  $t/\xi$  is decreased is consistent with the results of Hsiang and Finnemore<sup>54</sup> for Pd-Cd-Pb sandwiches, for which  $t \approx \xi_N$ .

Using Eqs. (8) and (12), we adapt the flux-pinning model of Gurevich and Cooley<sup>29</sup> for planar pins having zero thickness in order to encompass proximity coupling of pins hav-

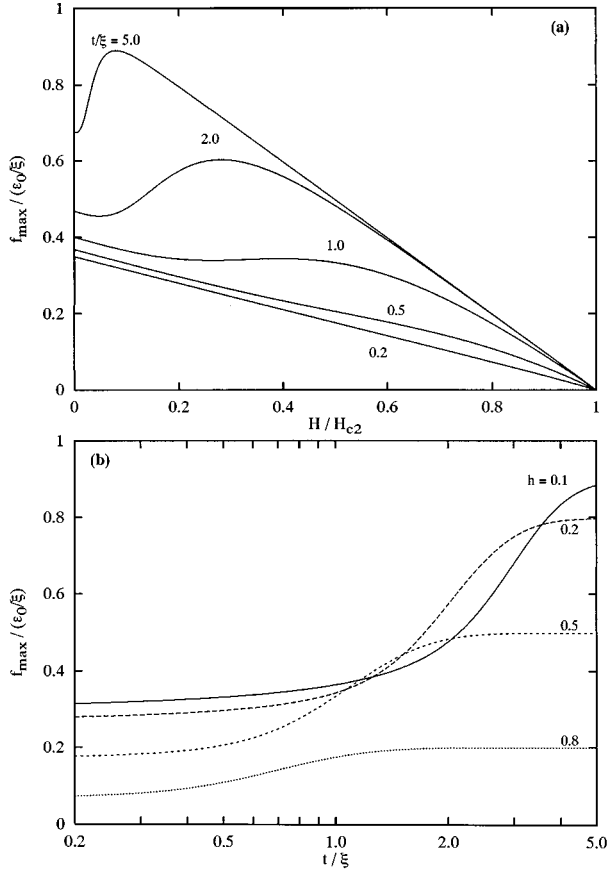


FIG. 2. Model elementary pinning force. (a) Field dependence of the magnetic pinning force for various values of  $t/\xi$ . A factor of  $(1-H/H_{c2})$  multiplies all of the curves to account for the field dependence of the superconducting order parameter. (b) Dependence of the magnetic pinning force on  $t/\xi$  for various reduced fields.

ing  $t \sim \xi_N$ . The elementary pinning force, given by Eq. (5), then takes on a direct dependence on  $j_p(H, T, t) \equiv J_p(H, T, t)/J_0(T)$ :

$$f_{\max} \approx -\frac{\epsilon_0}{\xi} \left[ \frac{1}{1+j_p} - \frac{2j_p}{(2j_p+1)^2} \right]. \quad (13)$$

We assume that an additional factor of  $(1-h)$  appears in the field dependence of  $f_{\max}$  to account for the reduction of the superconducting order parameter. Also, the contribution of core pinning,  $f_p = 0.22(\epsilon_0/\xi)(1-h)$ ,<sup>40</sup> should be added to Eq. (13). The total elementary pinning force, expressed as a function of  $h$  at fixed temperature and pin thickness, is then given by

$$f_p(h) = (1-h) \frac{\epsilon_0}{\xi} \left\{ 0.22 + \left[ \frac{1}{1+j_p(h)} - \frac{2j_p(h)}{(2j_p(h)+1)^2} \right] \right\}. \quad (14)$$

This elementary pinning force is plotted as a function of  $H/H_{c2}$  for different pin thicknesses in Fig. 2(a), and as a function of  $t/\xi$  (not  $t/\xi_N$ ) for different reduced fields in Fig. 2(b). In Fig. 2(a),  $f_{\max}$  attains a local maximum at a reduced

field slightly higher than  $H_d/H_{c2}$  ( $\xi_N = 3.3\xi$  in the plots). This corresponds to a rapid increase of  $l$  caused by the exponential decrease of  $J_p$  when  $H > H_d$ . The increase of  $l$  brings about a crossover from the nonlocal to the local regime of the pinning mechanism, which results in an increase of order  $\ln\lambda/\ln l$  in  $f_{\max}$ . The appearance of the maximum in  $f_{\max}(h)$  immediately suggests that an unconventional *bulk* pinning force curve should be obtained. Further, the crossing of the lines near  $t/\xi = 1$  in Fig. 2(b) indicates a shift in the position of the peak of the bulk pinning force curve as  $t/\xi(T)$  is changed. This shift destroys temperature scaling and produces a change in the shape of  $F_p(H)$  at constant temperature as the pin thickness varies. This vital point will be discussed further in Sec. II D.

### C. Effect of decoupling on the number density of flux-pinning interactions

Direct summation implies that the elementary pinning force can be multiplied by the number density of flux-pinning interactions  $n$  to give the bulk pinning force.  $n$  is limited by the number density of *fluxons* when there are fewer fluxons than pins and by the number density of *pins*  $n_p$  at higher fields. This suggests that the summation should be linear in field at low field,  $n \propto H$ , and independent of field at high field,  $n \sim n_p$ .

However, at a characteristic field

$$\mu_0 H \approx \frac{\phi_0}{[l(H, T, t)]^2}, \quad (15)$$

the phase kinks of the *AJ* vortices *overlap*, breaking the phase coherence across the planar pin.<sup>30</sup> No more *AJ* vortices can be added to the pins for  $H > H_l$ . The field  $H_l$  is close to  $H_d$  and is related to the decoupling of the pins (the difference between  $H_l$  and  $H_d$  is  $< 0.05H_{c2}$  for  $0.2 < t/\xi_N < 2$ ).

The phase difference along  $x$  across the contact gives rise to a current  $j_s$  which flows parallel to the contact. The Lorentz force of this current is identical to the pinning force of the contact on the overlapping *AJ* vortices. But, because the pins are assumed to have uniaxial alignment,  $j_s$  flows parallel or antiparallel to the transport current. The pins thus behave like internal surface barriers.

Thus, we cut off the regime of linear summation at  $H_l$ , instead of at  $\mu_0 H \approx n_p \phi_0$ . When  $H \gg H_l$ , we have  $n \approx \mu_0 H_l / \phi_0$  from the interpolation formula

$$n = \frac{\sqrt{(\mu_0 H)^2 + (\mu_0 H_l)^2}}{\phi_0}. \quad (16)$$

### D. The shape of the bulk pinning force curve

Bulk pinning force curves derived by combining Eqs. (14) and (16),  $F_p = n f_p$ , are shown in Fig. 3. Optimization of both the magnitude of  $F_p$  and the position of the maximum in the pinning force curve  $F_{\max}$  is seen in plots (a)–(c), where the pin thickness is changed. In plots (a) and (b) the pin thickness ranges from  $0.2\xi$  to  $5\xi$  and we take  $\xi_N = 6.6\xi$  and  $3.3\xi$ , respectively. In plot (c) the pin thickness ranges from  $0.1\xi$  to  $2\xi$  and we take  $\xi_N = \xi$ . Figures 3(a)–(c) clearly

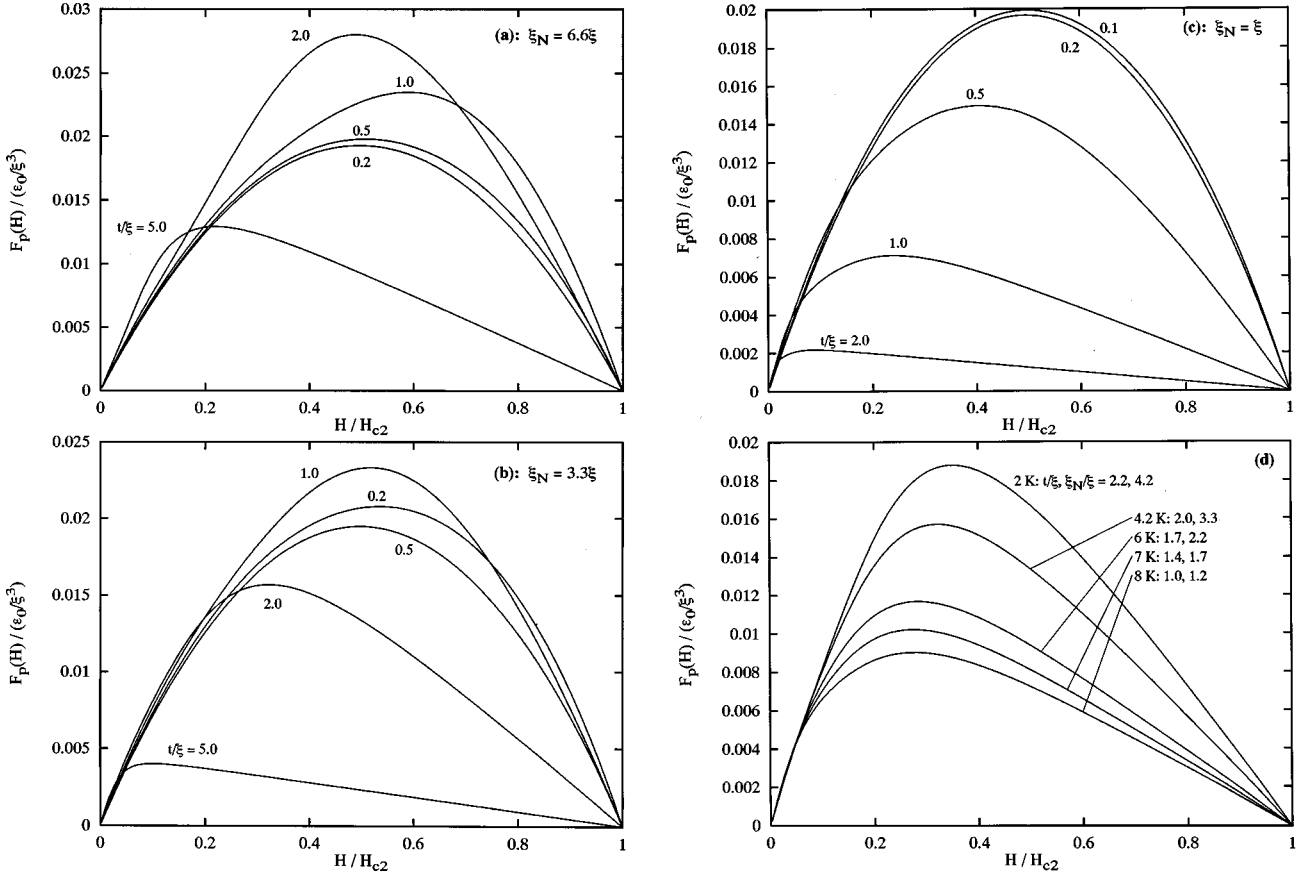


FIG. 3. Bulk pinning force curves predicted by the flux-pinning model. (a)–(c)  $F_p(H)$  curves as a function of reduced field for various values of  $t/\xi$ . The value of  $\xi_N$  is  $6.6\xi$  in (a),  $3.3\xi$  in (b), and  $1.0\xi$  in (c). (d) Simulation of the lack of temperature scaling of  $F_p(H)$ . The curves are labeled by the pairs  $t/\xi(T)$ ,  $\xi_N/\xi(T)$  for  $t=2.3\xi(0)$  and  $\xi_N(T_c)=2.5\xi(0)$ . The temperature dependence of  $\xi(T)$  is proportional to  $[1 - (T/T_c)^2]^{-1/2}$ .

show how the peak of  $F_p(h)$  moves toward higher field and becomes higher in magnitude as  $t$  decreases to its optimum value,  $t_{\text{opt}} \sim \xi_N/3$ , except in plot (c), where  $t_{\text{opt}} \sim \xi_N/10$ . The magnitude of  $F_p$  decreases and the shape of the  $F_p(H)$  curve saturates when  $t < t_{\text{opt}}$ . The optimum curves represent the best balance between summation and the elementary pinning force. In particular, plot (c) shows a smaller value of  $t_{\text{opt}}$ , because  $H \sim H_{c2}$  and the number density of pins is very high. The shape of the saturated  $F_p(H)$  curves [ $t/\xi=0.2$  and  $0.5$  in plot (a),  $0.5$  in plot (b), and  $0.2$  and  $0.1$  in plot (c)] reflects our assumption that the elementary pinning force is proportional to  $(1-h)$ .

Figure 3(d) explicitly shows the lack of temperature scaling. The plots are labeled by the values  $t/\xi(T)$ ,  $\xi_N(T)/\xi(T)$ , where we chose  $t=2.3\xi(0)$  and  $\xi_N(T_c)=2.5\xi(0)$ . The sequence of curves, beginning with the curve labeled 2.2, 4.2, thus corresponds to the temperatures 2, 4.2, 6, 7, and 8 K with  $T_c=9$  K,  $\xi(0)=4.8$  nm,  $\xi_N(T_c)=12$  nm, and  $t=11$  nm. We use the standard temperature dependence  $\xi(T) \propto [1 - (T/T_c)^2]^{-1/2}$ . As the temperature is increased, the value of  $t/\xi$  increases relative to that of  $\xi_N/\xi$ , and the peaks of the curves move toward lower field. Partly, the movement of the peaks occurs because the value of  $t/\xi_N(T_c) \approx 1$ , so the curves become less nearly optimum as  $T$  increases. If instead  $t/\xi_N(T_c)$  were only 0.1, the curves would become more nearly optimum as  $T$  increases, and

their peaks would move slightly toward higher field [see Figs. 3(a) and (b)]. They would then exhibit scaling.

### III. EXPERIMENT

#### A. Composite fabrication and estimation of pin thickness

An outline of the fabrication and microstructure of the APC composite appears in Ref. 15. We present additional TEM data in this paper in order to define the pin thicknesses at the small filament diameters used in the experiment.

To summarize the fabrication process for the composite, round Nb1Ti pins were inserted into a hexagonal array of 61 holes drilled parallel to the axis of a round Nb47Ti ingot, the superconducting matrix, as schematically shown in Fig. 4(a). This composite Nb47Ti/Nb1Ti billet was extruded from a diameter of  $\sim 150$  mm to a diameter of  $\sim 80$  mm. All subsequent processing was by wire drawing at room temperature, thus minimizing thermal mixing of the components at smaller wire diameters. The composite filaments were drawn in a copper matrix, using two 61-element and one 7-element restacking stages to achieve the necessary diameter reduction. Wire samples used in the experiment thus contained 3721 or 26047 Nb47Ti filaments.

TEM images show uniform arrays of round pins at pin thicknesses (diameters)  $\geq 92$  nm.<sup>15</sup> For smaller filament diameters, as seen sequentially in Figs. 4(b)–(e), the pins

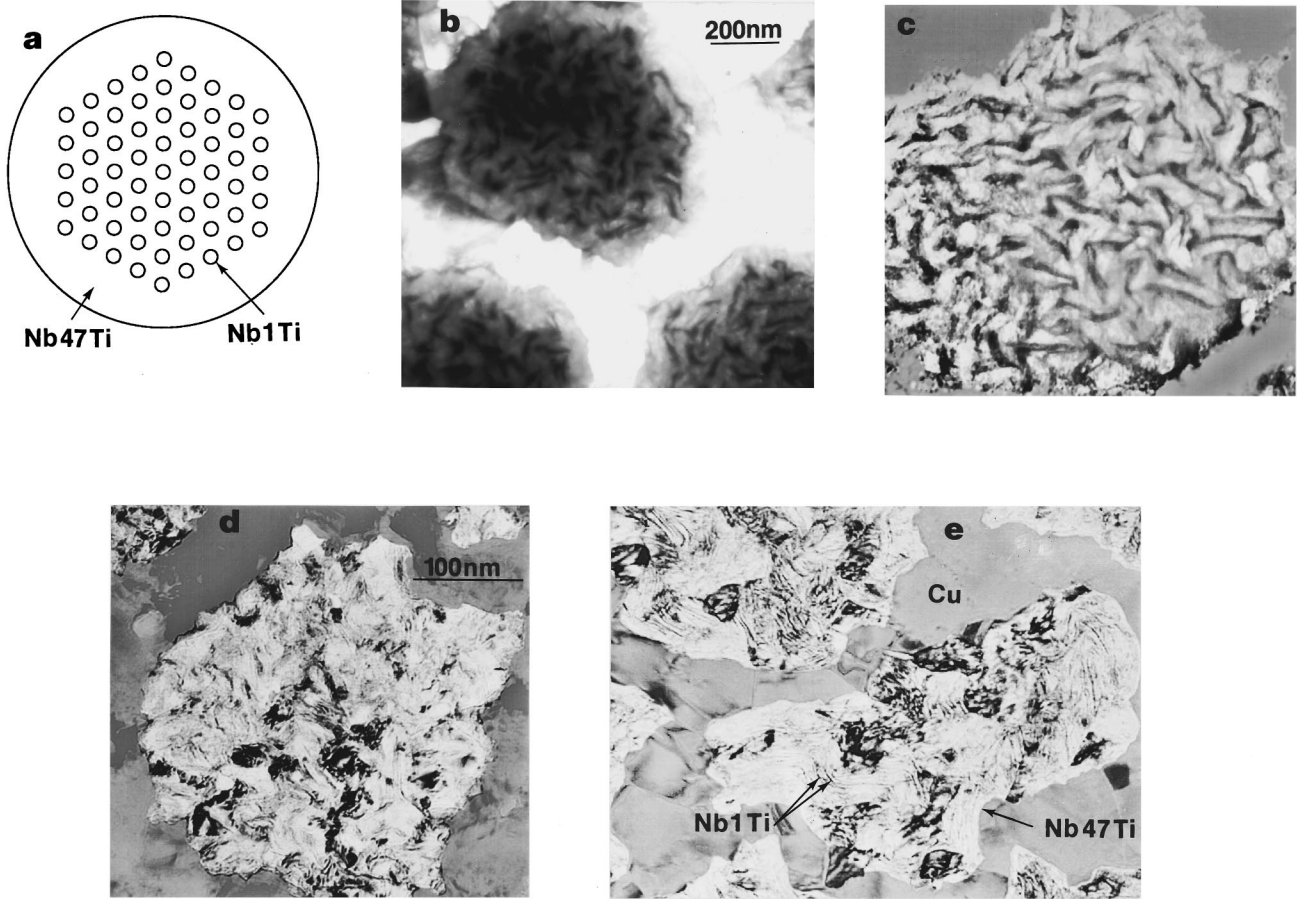


FIG. 4. The microstructure of the APC wire. (a) A sketch of the Nb47Ti superconductor and Nb1Ti pin array cross section. (b)–(e) Transmission electron microscopy of the superconductor and pin array, for  $t = 14$  nm (b), 11 nm (c), 4.8 nm (d), and 1.8 nm (e). The pins, superconductor, and copper matrix are labeled. The micrographs in (c)–(e) have been digitally enhanced to more clearly define the filaments and the pins. Micrographs (b)–(c) and (d)–(e) have the same magnification.

themselves are no longer round and instead develop an aspect ratio that increases with decreasing filament diameter. We determined  $t$  for Figs. 4(b) and (c) by first tracing the shapes of the pins on plastic foils placed over enlargements of the TEM images.<sup>26</sup> This resulted in a binary image, from which digital analysis could be performed. We then used the algorithms of Lee, Larbalestier, and Jablonski<sup>31</sup> to analyze the binary images. We found a similar relationship between  $t$  and filament diameter as found between  $\alpha$ -Ti precipitate thickness and wire diameter by Meingast, Lee, and Larbalestier.<sup>7</sup> In terms of  $d_f$ , this relationship is

$$t = 100 \left( \frac{d_f}{2000} \right)^{1.6}, \quad (17)$$

where  $t$  and  $d_f$  are in nanometers. The relationship in Eq. (17) is reasonable because the fitting parameter, 100 nm, is close to the diameter of the smallest round pins observed by TEM, 92 nm. We use this expression to estimate  $t$  for the smaller wire diameters, and general agreement is found between Eq. (17) and Figs. 4(d) and (e). Also, Eq. (17) indi-

cates that filament diameters approach the magnetic penetration depth,  $\sim 250$  nm, when the pin thickness is a few nanometers.

### B. Transport flux-pinning measurements

The bulk pinning force of the Nb47Ti/Nb1Ti APC wires was determined at 4.2 K by transport measurements, where

$$F_p(H) = J_c(H) \mu_0 H. \quad (18)$$

The critical current was determined by a four-point resistance measurement at a resistive criterion of  $10^{-14} \Omega \text{ m}$ .  $J_c$  was then obtained by dividing the critical current by the total cross-sectional area of the superconductor. The area of the superconductor was determined by weighing a known volume of wire for which the densities of all of its components were known. The transport experiment was carried out under a liquid helium bath at nominally 101.3 kPa (760 Torr) pressure, such that the sample holder shared a common center and axis with a long superconducting solenoid capable of 10 T. The digital measurements of the voltage as a function of

current were highly reproducible; the standard error for a Nb-Ti standard wire (NIST SRM No. 1457) was less than 1 part in  $10^4$ .

The  $F_p(H)$  curves have a significant contribution from surface pinning at small filament diameters, as discussed in the next section. The maximum bulk pinning force attained was  $23 \text{ GN/m}^3$  at 2.5 T.

### C. Magnetization flux-pinning measurements

The bulk pinning force at temperatures other than 4.2 K was determined by magnetization measurements. We used the Bean model<sup>55</sup> to determine  $J_c$ ,  $J_c = 3\pi\Delta M/4d_f$ , where  $\Delta M$  is the magnetization difference between the field-descending and the field-ascending branches of the  $M(H)$  hysteresis loop and  $d_f$  is the filament diameter. The  $F_p(H)$  curves were obtained using Eq. (18). The magnetic moment was measured using a vibrating sample magnetometer (VSM) with the filaments perpendicular to the field. The samples were contained within a variable-temperature He gas atmosphere, in which control over the sample temperature could be established between 2 and 12 K with a precision of not less than 50 mK. The absolute error of the temperature was 2%.

Magnetization experiments on multifilament wire samples can be difficult to interpret because of the flow of current across the copper matrix. In order to avoid this problem, extracted filaments were used. Depending on the wire diameter, 4–16 pieces of the long samples used for the transport measurements were bundled in parallel alignment, placed under tension, and then immersed in a nitric acid bath in order to etch away residual solder and the copper matrix. The tension ensured that the filaments remained straight and parallel. The acid solution was then rinsed away, and the filaments were immediately placed in a dilute solution of celluloid cement in acetone. The low viscosity of the solution allowed most of the  $10^5$ – $10^6$  filaments to be coated with cement, protecting them from further oxidation. This resulted in a 1–2 cm long bundle of straight filaments with masses of 5–10 mg. We took steps to ensure that there were no superconducting loops created by crossed filaments.

In order to compensate for operational errors, errors in applying the Bean model to small filament diameters, and errors in the sample volume, the  $F_p(H)$  data were then scaled so as to make equal the transport and magnetization  $F_p(H)$  curves at 4.2 K. This scaling factor was then applied to the data at other temperatures. The normalization changed the data by 17% in one case, and by less than 9% for all other samples.

## IV. RESULTS

### A. Parameters of the superconducting state

We analyze our experimental data in terms of the ratio  $t/\xi(T)$ , where  $\xi(T)$  is the coherence length. We determined  $\xi$  by measuring  $H_{c2}(T)$  and applying

$$\xi(T) = [\phi_0/2\pi\mu_0 H_{c2}(T)]^{1/2}. \quad (19)$$

$H_{c2}(T)$  was determined by the field at which the magnetization hysteresis was extrapolated to zero. Values of  $\mu_0 H_{c2}(T)$  as a function of average pin thickness are given in

TABLE I. The upper critical field as a function of pin thickness at the temperatures examined.

$d_f$ (nm)	$t$ (nm)	$\mu_0 H_{c2}$ (T)					
		2 K	4.2 K	6 K	7 K	8 K	8.5 K
Bulk		13.3	11.0	7.8	5.0	2.5	1.3
840	25	12.6	10.6	7.2	4.6		
580	14	12.3	10.0	7.1	4.4	2.0	1.1
500	11	12.0	9.7	6.8	4.2	2.0	1.2
400	7.6	12.0	9.4	6.5	4.1		
300	4.8	11.8	9.2	6.4	4.2	2.1	1.2
220	2.9	11.7	9.0	6.4	4.2		
196	2.5		8.9				
174	2.1		8.9				
154	1.8		8.8				
140	1.5		8.8				

Table I. To increase confidence in these values, we compared them to  $H_{c2}$  values obtained by two other procedures: (1) a linear extrapolation to zero of the magnetization observed after cooling in field, using a VSM at low temperatures and a superconducting quantum interference device magnetometer at high temperatures; and, (2) an extrapolation of the bulk flux pinning force to zero. Generally, these values fell within  $\pm 3\%$  of the values listed in Table I.

The Ginzburg-Landau parameter  $\kappa$  was determined from the linear variation of  $H_{c2}(T)$  near  $T_c$  using the formalism of Orlando *et al.*<sup>56</sup> Values of  $\kappa$  are given in Table II. They are only weakly dependent on pin thickness,  $40 < \kappa < 48$ , and are centered around the value for bulk Nb47Ti,  $\kappa = 43$ . The magnetic penetration depth was then found by using

$$\lambda(T) = \kappa \xi(T). \quad (20)$$

Penetration depth values were compared against penetration depths extracted from the field at which deviation from perfectly diamagnetic behavior was noted for a sample cooled in zero field, with good agreement.

For all samples,  $9 < T_c < 9.3 \text{ K}$ .

### B. Surface pinning

The magnetic interaction between the fluxons and their images is enhanced when  $d_f \sim \lambda(T)$ .<sup>38,39,57–59</sup> This enhanced magnetic interaction leads to several effects, among which is strong flux pinning by the filament surfaces at fields below the critical field

$$H_c(d_f, T) \approx H_{cB} \frac{\lambda}{d_f}. \quad (21)$$

Although still much smaller than  $H_{c2}$ ,  $H_c(d_f, T)$  can be substantially higher than the bulk value of the critical field,

TABLE II. The values of the Ginzburg-Landau parameter as a function of pin thickness.

$t$ (nm)	$\infty$	25	14	11	7.6	4.8	2.9	2.5	2.1	1.8	1.5
$\kappa$	43	45	48	40	41	42	42	42	42	42	42

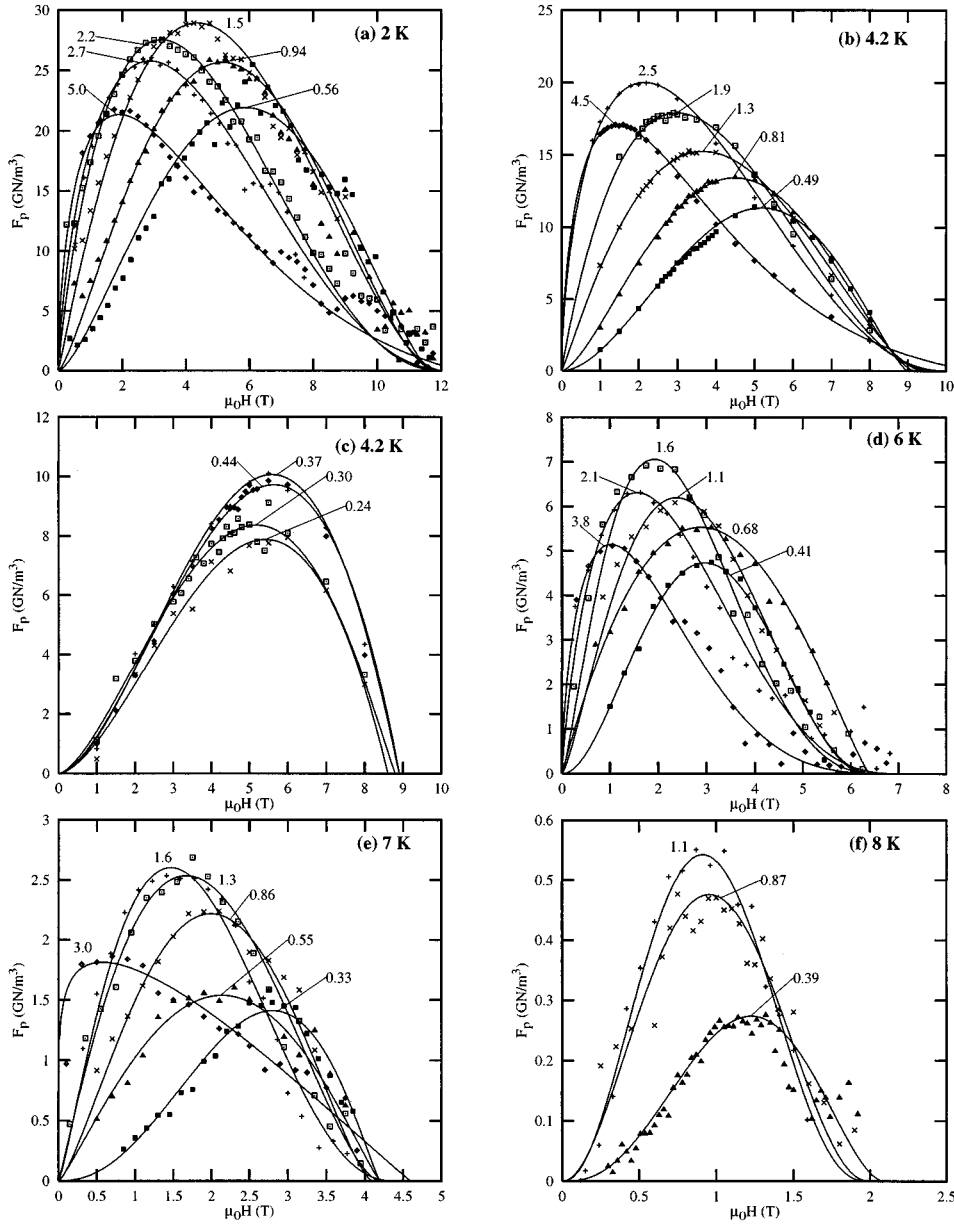


FIG. 5. Bulk pinning force curves after adjustment for surface pinning. (a) 2 K; (b) and (c) 4.2 K; (d) 6 K; (e) 7 K; (f) 8 K. The curves are labeled by the value of  $t/\xi(T)$ , and the labels are placed near the peak of their respective curves. The data at 2, 6, 7, and 8 K have been thinned to keep the plots clear. The solid lines are least-squares fits of a function  $F_p(H) = Ch^p(1-h)^q$ , where  $h = H/H_{c2}$ .

$$H_{cB} = \frac{\phi_0}{2\sqrt{2}\pi\lambda\xi\mu_0}, \quad (22)$$

where  $\mu_0 H_{cB} \approx 0.18$  T at 4.2 K.

We measured APC wires having filament diameters as small as  $\lambda$  (4.2K). In order to deduce the flux pinning due only to the pins, we subtracted the total pinning force due to the filament surfaces,

$$F_s(H, T, d_f) = \mu_0 H J_s(H, T, d_f), \quad (23)$$

from the measured  $F_p(H, T, t)$  data, where  $J_s$  is the critical current density due to surface pinning.  $J_s$  was determined by measuring the critical current of an identically fabricated composite wire containing only pure Nb47Ti filaments without the APC array, for which we assumed surface pinning

was the dominant pinning mechanism when  $d_f < 2\lambda$ . We found<sup>26,60</sup> that  $J_s$  diverged at low fields and  $\lim_{H \rightarrow 0} F_p(H) \neq 0$ , which is not predicted by existing models of surface pinning.<sup>38,58,59</sup> An empirical formulation of  $J_s(h, T, d_f)$  was instead obtained,<sup>60,61</sup>

$$J_s(h, T, d_f) = \frac{H_{cB}(T)}{\sqrt{2}\kappa d_f} \frac{(1-h)\ln(1/h)}{\sqrt{h}} + J_L, \quad (24)$$

where  $J_L = 6 \times 10^8$  A/m<sup>2</sup> is a background bulk current density due to all other pins, determined when  $d_f \gg \lambda$ . The  $F_s(H)$  curve based on this equation has a peak at very low fields ( $h = 0.086$ ).

TABLE III. Fitting parameters  $p$  and  $q$  for the  $F_p(H)$  data.

$t/\xi(T)$	$p$	$q$	$h_{\text{peak}}=p/(p+q)$
2 K: <sup>a</sup>			
2.7	0.70	2.30	0.23
2.5	0.85	2.30	0.27
1.5	1.04	1.82	0.36
0.94	1.35	1.74	0.44
0.56	1.49	1.47	0.50
4.2 K: <sup>a</sup>			
2.5	0.59	2.08	0.22
1.9	0.93	2.08	0.31
1.3	1.08	1.69	0.39
0.81	1.55	1.63	0.49
0.49	1.90	1.40	0.58
0.44	1.68	0.97	0.63
0.37	1.76	1.04	0.63
0.30	1.60	1.12	0.59
0.24	1.70	1.02	0.63
6 K:			
3.8	0.63	3.80	0.14
2.1	0.83	2.93	0.22
1.6	1.31	3.30	0.28
1.1	1.35	2.33	0.37
0.68	1.02	1.22	0.46
0.41	2.05	2.38	0.46
7 K:			
3.0	0.15	1.05	0.13
1.6	1.25	2.50	0.33
1.3	1.10	1.67	0.40
0.86	1.40	1.48	0.49
0.55	1.21	1.17	0.51
0.33	2.40	1.20	0.67
8 K:			
1.1	2.35	2.81	0.46
0.87	2.10	2.30	0.48
0.39	2.80	2.00	0.58

<sup>a</sup>Fits could not be obtained for  $t=25$  nm at 2 K ( $t/\xi=5.0$ ) and 4.2 K ( $t/\xi=4.5$ ).

### C. Reduced $F_p(H)$ curves

When combined with bulk pinning in our APC wires, surface pinning caused  $F_p$  to approach a *finite value* as  $H \rightarrow 0$  for small filament diameters. The intercept at  $H=0$  increased as  $d_f/\lambda$  decreased, indicating the larger contribution of surface pinning for smaller filament diameters.

However, after subtracting  $F_s$  according to Eqs. (23) and (24), more conventional shapes of the bulk pinning force curves were obtained. The resulting  $F_p(H)$  data are presented as six plots in Fig. 5. Plots (a)–(f) correspond to temperatures between 2 and 8 K, as shown on the plots. The values of  $t/\xi(T)$  are labeled near the corresponding curve. Plot (c) presents data obtained only at 4.2 K for wires which were too small to measure magnetically. In each of these plots, the value of  $F_s(H)$  was subtracted in a pointwise manner from the  $F_p(H)$  curves obtained in the previous section. The value  $\mu_0 H_{cB} = 0.237[1 - (T/T_c)^2]$  T was used to determine  $J_s$ . The solid lines are least-squares fits to a function  $F_p(H) = Ch^p(1-h)^q$ , where  $p$  and  $q$  are listed in Table III

and  $C$  is a constant.

The adjusted  $F_p(H)$  curves have typical shapes for bulk flux-pinning force curves. The individual curve shapes and the evolving curve shape as the value of  $t/\xi$  becomes smaller resemble  $F_p$  data reported for other Nb-Ti/Nb APC composites with filament diameters much larger than  $\lambda$ .<sup>23–25</sup> The curves that received the largest correction are those shown in Fig. 5(c). However, these are consistent with the unusual curves obtained from composites with very thin pins and large filament diameters, as reported by Matsumoto *et al.*<sup>23</sup> and Heussner *et al.*<sup>24</sup> In these two reports, the peaks of the  $F_p(H)$  curves reached fields as high as  $0.66H_{c2}$ . Thus we believe that our method of subtraction of the surface pinning is justified.

The curves obtained from magnetization measurements were somewhat noisy. This is partly due to the small volume of the samples, for which  $m \leq 10^{-7}$  A m<sup>2</sup> at high field. However, we also observed oscillations of  $F_p(H)$  on the order of 3% of the magnitude of  $F_{\text{max}}$ , previously described in Ref. 16. These oscillations do not appear here, only because every fifth data point is plotted. Some data points lie at the peaks and others at the valleys of the oscillations.

Finally, we note that the  $F_p(H)$  curves in Fig. 5 exhibit a clear variation of shape as a function of  $t/\xi$ . The trend is first for the curves to increase in magnitude by increasing the field at which the peak value of  $F_p$  is attained, as the pin thickness is reduced. After  $F_p$  reaches its maximum as a function of  $t$ , the curves continue to peak at ever increasing reduced fields. An optimum curve can be distinguished in Figs. 5(a), (b), (d), and (e). The optimum value of  $t/\xi$  lies between 1.5 and 2.5, and becomes somewhat smaller as the temperature increases. A lack of temperature scaling, which is explicit in Fig. 6, is also evident. The data for  $t=4.8$  and 14 nm are plotted in reduced units in order to highlight the change in the shape of  $F_p(h)$ .

## V. DISCUSSION

### A. Comparison of the flux-pinning model and the experiment

There are important similarities between the experimental data presented in Sec. IV C. and the flux-pinning model described in Sec. II. First, the magnitudes of the bulk pinning forces are in agreement. Taking  $\epsilon_0 = 5 \times 10^{-13}$  N and  $\xi = 5$  nm, both values being appropriate for  $T=2$  K, the scaling value  $\epsilon_0/\xi^3$  in Fig. 3 is 4000 GN/m<sup>3</sup>. Thus, the model predicts maximum bulk pinning forces on the order of 10–100 GN/m<sup>3</sup> at 2 K, which encompasses the range of bulk pinning forces seen in the experimental data, 20–30 GN/m<sup>3</sup>.

The model also predicts quantitatively the optimization behavior for our APC conductor containing Nb1Ti pins. At each temperature, except for 8 K where the data are very limited, the experimental data show a clearly optimum  $F_p(H)$  curve. The value of  $t_{\text{opt}}/\xi$  generally decreases with increasing temperature: at 2 K,  $t_{\text{opt}}/\xi \approx 1.5$ –2.2; at 4.2 K, 2.5; at 6 K, 1.6; at 7 K, 1.3–1.6; and at 8 K,  $t_{\text{opt}}/\xi \geq 1.1$ . The decreasing value of  $t_{\text{opt}}/\xi$  as temperature increases is consistent with a roughly constant value of  $t_{\text{opt}}$ . Also, using the relationship  $t_{\text{opt}} \sim \xi_N(T)/3$  from the flux pinning model, values of  $\xi_N(T_c)$  can be extracted. These are 12, 22, 14, 11, and

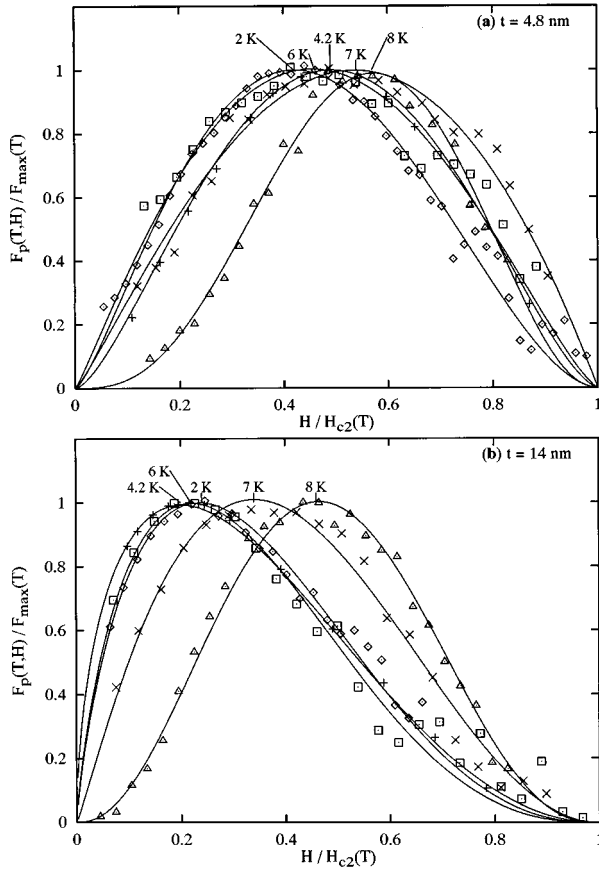


FIG. 6. The lack of temperature scaling of  $F_p(H)$ . Normalized bulk pinning force curves for 2 pin thicknesses are plotted as a function of the reduced field at different temperatures. The temperature labels are placed near the peak of their respective curves.

6.7 nm, respectively, from the 2–8 K values of  $t_{\text{opt}}/\xi(T)$  derived above. These average to 13 nm, which is very close to the dirty limit value of 11.9 nm calculated in Sec. II B.

The modeling of the evolution of the  $F_p(H)$  curve with pin thickness in Figs. 3(a)–(c) has the same trends seen in the experimental data, although the exact curve shapes agree less well. The optimum  $F_p(H)$  curves in Figs. 3(a)–(c) all have peaks near  $h=0.5$ , while the optimum experimental curves have peaks near  $h=0.3$ . We think that the lack of agreement is primarily a consequence of assuming that  $f_p$  has a field dependence proportional to  $(1-h)$ , a point which we discuss further in Sec. V B. Other potential sources of the difference in  $F_p(H)$  curve shape are the interpolation formulas for  $J_p$  and  $n$ . Nonetheless, we find consistent agreement between the position of the reduced field  $h_{\text{peak}}=p/(p+q)$  and the value of  $H_d/H_{c2}$ , as shown in Fig. 7. Since the value of the decoupling field approximately locates the local maximum of the elementary pinning force at  $H>0$ , the reduced field  $H_d/H_{c2}$  should approximate the positions of the peaks of the fitted curves. The values of  $h_{\text{peak}}$  are listed in Table III, and are plotted along with the line given by  $H_d(T,t)$  for  $\xi_N=3.3\xi$  in Fig. 7. The experimental data points fit the model rather closely.

The lack of temperature scaling that appears in the experimental data is somewhat consistent with the flux-pinning

model. The model predictions in Fig. 3(d) show the peak in  $F_p(h)$  shifts toward lower field as the temperature increases when the pin thickness is greater than optimum. However, there can also be a shift toward higher field with a temperature increase when the pins are thinner than optimum, as can be deduced from the sequence of plots in Figs. 3(a)–(c) for  $t/\xi=0.5$  and 1.0. In the experimental data, we noticed a somewhat stronger shift toward higher field than predicted by the model, both when  $t\approx\xi(0)$ , as shown in Fig. 6(a), and when  $t\approx\xi_N(T_c)$ , as shown in Fig. 6(b). Also, scaling appeared to hold for  $T<7$  K. The slight difference between the model predictions and the experimental data may be due to the fact that Nb1Ti pins are superconducting. In this case the proximity length can increase with increasing temperature over a limited range of temperature, instead of having the temperature dependence given by Eq. (6). To support this conjecture, we note that the shift predicted by the model is seen in TMP Nb-Ti wires having  $\alpha$ -Ti precipitates of shorter  $\xi_N$ ,<sup>8</sup> and for which  $T_{cN}$  of the  $\alpha$ -Ti pins is  $\sim 1$  K.

Finally, we find consistency between the model and the experiment in the temperature dependence of the bulk pinning force.  $F_p(T)$  should be proportional to  $J_0(T)/\xi(T)$ , and since  $J_0(T)\propto(1-T/T_c)^2\sim[H_{c2}(T)]^{2.0}$  and  $\xi(T)\propto[H_{c2}(T)]^{-0.5}$ , we should observe  $F_p(T)\propto[H_{c2}(T)]^{2.5}$ . This is indeed seen. In Fig. 8 we plot the maximum value of  $F_p$  against the value of  $H_{c2}(T)$  for the data in Fig. 5. The slope of the line drawn through the data is equal to 2.5. We chose to plot data at the maximum of the  $F_p(H)$  curve because similar proximity coupling conditions should apply for all of the curves. We have already shown in Fig. 7 that the peaks of the curves lie close to the line given by the decoupling field.

## B. Validity of the model

We assumed that the order parameter in the superconductor decreases with increasing field as  $(1-h)$ , giving  $f_p\propto(1-h)$ . A more appropriate expression may in fact be  $f_p\propto(1-h)^2$  since this takes into account the magnetic energy of the whole vortex lattice.<sup>4</sup> However, this conjecture cannot be explicitly asserted because of the need to consider simultaneously ensembles of pinned  $AJ$  vortices, unpinned  $A$  vortices, and many proximity-coupled planar defects. As yet, no treatment of this complex situation has been presented.

In the absence of such a complete treatment, we therefore adopt the simplest assumption which permits a clear interpretation of the model. Here the single-fluxon treatment of the elementary pinning interaction does not include interactions of  $A$  and  $AJ$  vortices near a given pinned  $AJ$  vortex. In principle these must be considered in a complete treatment. However, since the effective magnetic range of the pins is  $l$ , rather than  $\lambda$ , the overlap is minimal when  $H<H_l$  or when the pin separation is greater than  $l$ . These two conditions oppose each other: when the pin separation is large,  $H_l$  is low, and vice versa. We therefore expect some disagreement between the experimental results and the model when  $h\geq 0.7$  for all pin thicknesses. At high fields, the overlap of the potentials of pins which are separated by less than  $l$  and the subsequent interaction of  $AJ$  vortices will reduce the pinning force.

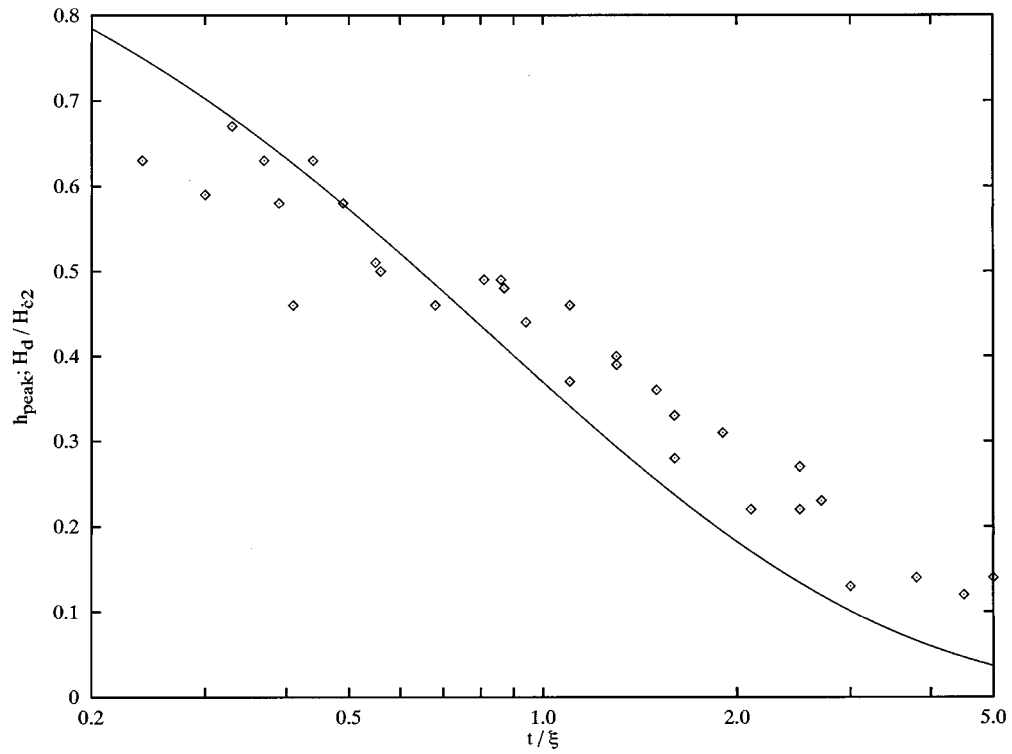


FIG. 7. Comparison of peak bulk pinning forces. The reduced field where the experimental bulk pinning force curves peak,  $h_{\text{peak}}$ , and the reduced decoupling field are plotted as functions of  $t/\xi$ . The data points are determined by the value of  $p/(p+q)$  for the fit curves, listed in Table III. The decoupling field, represented by the solid curve, is evaluated for  $\xi_N=3.3\xi$ .

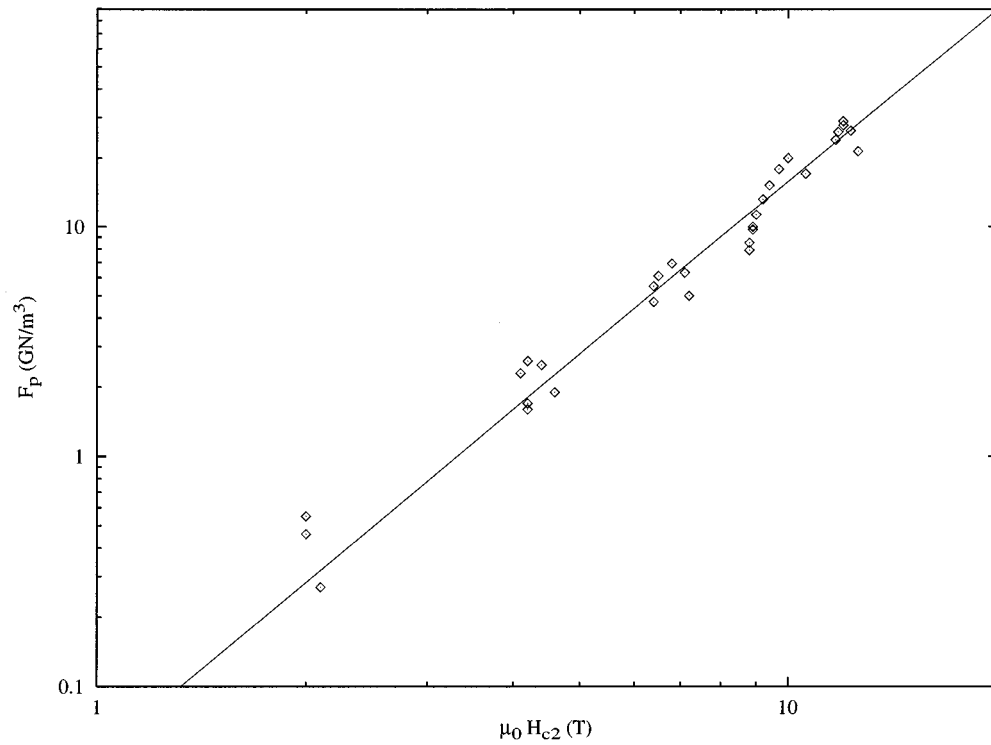


FIG. 8. The maximum bulk pinning force as a function of the upper critical field for the experimental data. The line represents  $F_p \propto [B_{c2}(T)]^{2.5}$ .

### C. The lack of temperature scaling

Major advances in the understanding of flux-pinning mechanisms occurred when Fietz and Webb<sup>32</sup> emphasized the temperature scaling of the bulk flux-pinning force in strong pinning systems. Such behavior is common in superconductors other than Nb-Ti. For example, scaling was observed in Nb 1–5 % Ti alloys,<sup>32</sup> in A-15 compounds,<sup>62</sup> in NbN,<sup>63</sup> and in high-temperature superconductors.<sup>64</sup> Classical flux-pinning theories incorporate scaling as a general property of flux-pinning systems with one dominant microstructural defect and pinning mechanism.<sup>4,20</sup> Scaling is a very powerful and useful idea: If it exists, it is sufficient to measure the shape of the bulk pinning-force curve at one convenient temperature in order to obtain detailed knowledge of the dominant pinning mechanism and its controlling microstructural defect.

The flux-pinning model developed is fundamentally different from such models because it predicts the *absence* of temperature scaling, even though there is one dominant microstructural defect. Lack of temperature scaling is a direct result of the high density of flux-pinning defects. At high pin number densities, the pin thickness must tend towards the proximity-coupled limit. The lack of scaling results because the proximity effect changes the *field* dependence of the elementary pinning force when the *temperature* is changed. This lack of temperature scaling occurs only when the pin thickness is of order  $\xi_N$ , but this is *exactly* the dense pin arrangement demanded by very high critical current density.

We discuss two examples in the literature concerning Nb-Ti superconductors below:

(1) Temperature scaling of  $F_p$  is not observed in Nb 44–62 wt % Ti. In the work of Meingast, Lee, and Larbalestier,<sup>7,8</sup> discussed in Sec. I, the lack of scaling at large wire diameter was attributed to pinning by both precipitates and grain boundaries. At optimum wire diameter, a lack of temperature scaling of  $F_p$  was again observed, even though the precipitate number density was an order of magnitude larger than that of the grain boundaries. Meingast, Lee, and Larbalestier puzzled over this inconsistency and in the end hypothesized that this could be explained by flux-pinning by *clusters* of precipitates. Clusters needed to be invoked because the diameter of the fluxon core at 8.5 K was three times the diameter at 4.2 K and approximately equal to the span of precipitate clusters observed by TEM. However, the concept of a precipitate cluster is unclear. In the context of the present model, the precipitate thickness passes through  $\xi_N$  as the temperature is raised, so different proximity coupling conditions exist at different temperatures. Since  $H_d \propto \exp(-t/\xi_N)$  and  $J_p \propto (H/H_d) \exp(-H/H_d)$ , the field dependence of the elementary pinning force is not the same at different temperatures. This naturally leads to a lack of scaling of  $F_p(H)$ . Thus the uncertain concept of precipitate clusters is not needed in our model.

(2) Scaling has been observed in an optimized Nb-Ti/Nb APC composite having a microstructure which has been determined by TEM examination to be similar to that of a TMP Nb-Ti composite.<sup>17</sup> Although the  $F_p(h)$  curves did not strictly overlap, temperature scaling was observed within experimental error over the temperature range 2–8.5 K. It was again reasoned that pin clusters were the defects controlling the pinning mechanism. However, in this case the flux pin-

ning was thought to be by perturbations of  $\lambda$ , because  $F_p(h)$  was proportional to  $(1-h)^{3/2}$ . In the context of the present model, the pin thickness (1–2 nm) in the study of Ref. 17 would have been much less than  $\xi_N$  ( $\sim 12$  nm) at all temperatures. The decoupling field would then always be near  $H_{c2}$  and  $J_p$  would be  $\sim J_0$  for all fields. This implies that the elementary pinning force would not have any significant temperature-dependent proximity-effect contribution. The bulk pinning-force curves were nearly optimum because the volume fraction of pins was very high (50%).<sup>14</sup> Thus it is not necessary to invoke pin clusters to explain the properties in this case either.

### D. Optimization of flux pinning

The fundamental parameter of the flux-pinning model developed here is  $\xi_N$ . In the context of the model, the flux-pinning properties of *any* metal or alloy with planar pins should be predictable.

The prediction that the optimum pin thickness  $t_{\text{opt}} \approx \xi_N/3$  is strikingly different from classical vortex-core flux-pinning models, which suggest instead that  $t_{\text{opt}} \approx 2\xi$ . Our experiment concluded that  $\xi_N \approx 12(T_c/T)^{0.5}$  nm for Nb1Ti pins. Thus the experimentally determined optimum Nb1Ti pin thickness is fairly thick (4–8 nm) when compared to that of  $\alpha$ -Ti (1–2 nm). Because both the pin thickness and the pin separation reduce simultaneously with increasing wire-drawing strain, the optimum elementary pinning force for Nb1Ti occurs for a fairly large pin separation (15–30 nm) and a fairly low number density of pins. This produces the unfavorable low-field peak in the optimum  $F_p(H)$  curve. *It is for this reason that most APC composites have not yet reached the full potential that artificial, model pin distributions potentially offer.*

In TMP Nb-Ti composites, it is experimentally clear that the optimum pin separation of  $\alpha$ -Ti precipitates is about 5 nm.<sup>7,13</sup> In this case summation of a large number density of elementary flux-pinning interactions determines  $F_p(H)$ , which then develops a peak at mid-field. The finding of an optimum precipitate thickness of 1–4 nm at 4.2 K by Meingast, Lee, and Larbalestier<sup>7</sup> suggests that  $\xi_N(T_c) \sim 7$ –10 nm for  $\alpha$ -Ti. This is significantly smaller than the value used by Stejic *et al.*<sup>14</sup> in their numerical calculations of flux pinning in multilayers. Indeed, a crucial property of TMP composites is, in the context of our model, that there is  $\sim 6\%$  Nb dissolved in  $\alpha$ -Ti. In addition, oxygen probably segregates preferentially to the  $\alpha$ -Ti, further diminishing  $\xi_N$ .<sup>65</sup> We took  $\xi_N(T_c) = 7$  nm for  $\alpha$ -Ti, giving  $\xi_N(4.2) \approx \xi(4.2)$ , in Fig. 3(c) in order to predict the optimization of  $F_p(H)$  for  $\alpha$ -Ti pins. The  $F_p(H)$  curves indeed bear a close resemblance to the optimization behavior for TMP Nb-Ti.<sup>8</sup>

These two examples suggest that a pin material with a short proximity length is needed to provide strong high-field flux pinning in an APC Nb-Ti composite or multilayer thin film. The optimization behavior of such an APC composite would then be similar to Fig. 3(c) and would depend on the volume fraction of pins. The  $F_p(H)$  curve for  $t/\xi = 0.1$  in Fig. 3(c) suggests that  $F_p \sim 80$  GN/m<sup>3</sup> could be achieved if the pin number density could be made to be on the order of  $\mu_0 H_l / \phi_0$ . Since  $H_l \sim H_d \sim H_{\text{peak}} \sim 0.5 H_{c2}$ , the number density of pinning interactions is about  $0.5 \mu_0 H_{c2} / \phi_0$

$\approx 0.1/\xi^2$ . This gives a pin volume fraction of about 10%, assuming all of the pins are parallel to the field. The shapes and orientations of the pins in a round wire composite will, of course, be random, and the usual approximation is to assume that half of the pins will be in the perpendicular orientation. Thus, a volume fraction of pins near 20% will instead be required. It is interesting that this is the volume fraction of  $\alpha$ -Ti pins which can be developed in TMP Nb-Ti, and is significantly less than the pin volume fraction which can be put into APC composites.

### E. Raising $J_c$ of Nb-Ti wires

The present proximity-effect model answers many troublesome questions about TMP Nb-Ti composites. It appears to be in qualitative agreement with the flux-pinning results for all high- $J_c$  Nb-Ti composites. Moreover, it appears that the quantitative predictions of the model are in good agreement with experiments. It should therefore be possible to raise the  $J_c$  of real Nb-Ti composites by intelligent pinning-center design.

In APC conductors made so far, their guiding design principle has been to add *more* pins than can be readily obtained in a TMP composite. To do this, fabrication compromises have been a paramount design consideration. This leads to the selection of pins that are ductile and form strong mechanical bonds with the copper sheath and the Nb-Ti matrix. Pure bcc and fcc metals tend to be chosen, for which  $\xi_N$  is long. Optimization is then achieved for low number densities of pins, and  $F_p$  is weak at high fields. Indeed, the TEM data in this paper and elsewhere<sup>16,17</sup> do not indicate a significant increase in the *number density* of pins in optimized APC wires, as compared to the number density of  $\alpha$ -Ti precipitates in TMP composites,<sup>7,13</sup> even though the *volume fraction* of pins is 1.5 to 2 times *higher* in the APC composites.

By contrast, the experiment in this paper demonstrates that it is not necessary to increase the volume fraction of pins past  $\sim 20\%$  in order to achieve a strong bulk pinning force. Even for 15% pins,  $F_p$  was 18–20 GN/m<sup>3</sup> at optimum filament diameter. Partly, the apparent increase in efficiency of the pins is due to the pins being the dilute alloy Nb1Ti rather than a pure metal, for which the proximity length is shortened somewhat as compared to that of pure Nb. Nonetheless, no APC wire to date has incorporated a pin material with a proximity length comparable to or shorter than that of  $\alpha$ -Ti

precipitates. Accordingly, no APC wire has exceeded the performance of TMP Nb-Ti wires at high fields, where high critical current is most desperately needed.

Thus, APC designs which incorporate small volume fractions of concentrated alloy pins should be the next research step toward higher  $J_c$ . It is absolutely vital to push the limit of high-field critical current density, and this paper shows that this goal cannot be achieved unless *both* the elementary pinning force *and* the number density of pins are the highest they can be. This will not occur until short proximity-length pins are incorporated into APC composite designs.

## VI. CONCLUSIONS

We have proposed that *magnetic* pinning is the dominant mechanism for proximity-coupled ribbon-shaped pins. We found that temperature scaling does not occur, and that  $F_p(H)$  is a function of pin thickness at constant temperature, because changes in the proximity coupling of the pins to the superconducting matrix cause changes in the elementary magnetic flux-pinning force. Our experiments on Nb-Ti wires showed that the optimum bulk pinning force occurs when the pin thickness is approximately  $\xi_N/3$ . This value represents a balance between a high elementary pinning force and a high number density of flux-pinning interactions. Further, the peak of the optimum *bulk* pinning force curve occurs at low field when the proximity length is equal to several coherence lengths, as is found for APC Nb-Ti conductors made with pure Nb or Nb 1 wt % Ti pins. The peak of the optimum curve moves toward the mid-field range ( $H/H_{c2} \approx 0.5$ ) when the proximity length decreases, as occurs for TMP Nb-Ti conductors with  $\alpha$ -Ti precipitates. We conclude that Nb-Ti/Nb APC composites suffer from a lack of high-field pinning because the proximity length of pure Nb pins is too long. Thus, we predict that the way to attain the full potential of APC conductors is to alloy the pins so that  $\xi_N$  is reduced to a smaller and more optimum value.

## ACKNOWLEDGMENTS

We gratefully acknowledge discussions with I. Hlášnik, A. Gurevich, P. Jablonski, and R. Scanlan. The experimental portion of the work was funded by the U.S. Department of Energy, Division of High Energy Physics, at the University of Wisconsin. Additional funding to L.D.C. was provided by the National Research Council at NIST.

\*Also Department of Materials Science and Engineering and Department of Physics.

<sup>1</sup>V. V. Shmidt and G. S. Mkrtchyan, Usp. Fiz. Nauk **112**, 459 (1974) [Sov. Phys. Usp. **17**, 170 (1974)].

<sup>2</sup>E. H. Brandt, Phys. Lett. **77A**, 484 (1980).

<sup>3</sup>P. G. deGennes, *Superconductivity of Metals and Alloys* [Addison-Wesley, New York, 1989 (reprint); originally published by W. A. Benjamin, New York, 1966].

<sup>4</sup>A. M. Campbell and J. E. Evetts, Adv. Phys. **21**, 199 (1972).

<sup>5</sup>T. Matsushita and H. Küpfer, J. Appl. Phys. **63**, 5048 (1988).

<sup>6</sup>H. Küpfer and T. Matsushita, J. Appl. Phys. **63**, 5058 (1988).

<sup>7</sup>C. Meingast, P. J. Lee, and D. C. Larbalestier, J. Appl. Phys. **66**, 5962 (1989).

<sup>8</sup>C. Meingast and D. C. Larbalestier, J. Appl. Phys. **66**, 5971 (1989).

<sup>9</sup>I. Pfeiffer and H. Hillmann, Acta Metall. **16**, 1429 (1968).

<sup>10</sup>D. F. Neal, A. C. Barber, A. Woodcock, and J. Gidley, Acta Metall. **19**, 143 (1971).

<sup>11</sup>R. G. Hampshire and M. T. Taylor, J. Phys. F **2**, 89 (1972).

<sup>12</sup>A. W. West and D. C. Larbalestier, Adv. Cryogenic Eng. (Materials) **26**, 471 (1980); IEEE Trans. Magn. **19**, 548 (1983); D. C. Larbalestier and A. W. West, Metall. Trans. A **15**, 843 (1984).

<sup>13</sup>P. J. Lee and D. C. Larbalestier, Acta Metall. **35**, 2523 (1987); J. Mater. Sci. **23**, 3951 (1988).

<sup>14</sup>G. Stejic, L. D. Cooley, R. Joynt, D. C. Larbalestier, and S. Takács, Supercond. Sci. Technol. **5** (1S), 176 (1992).

<sup>15</sup>L. D. Cooley, P. J. Lee, D. C. Larbalestier, and P. M. O'Larey, Appl. Phys. Lett. **64**, 1298 (1994).

<sup>16</sup>P. D. Jablonski, P. J. Lee, and D. C. Larbalestier, Appl. Phys. Lett. **65**, 767 (1994).

- <sup>17</sup>L. D. Cooley, P. J. Lee, and D. C. Larbalestier, *IEEE Trans. Magn.* **27**, 1120 (1991).
- <sup>18</sup>E. V. Thuneberg, *Cryogenics* **29**, 236 (1989); E. V. Thuneberg, J. Kurkijarvi, and D. Rainer, *Phys. Rev. B* **29**, 3913 (1984).
- <sup>19</sup>W. E. Yetter, D. A. Thomas, and E. J. Kramer, *Philos. Mag. B* **46**, 523 (1982).
- <sup>20</sup>E. J. Kramer, *J. Appl. Phys.* **44**, 1360 (1973).
- <sup>21</sup>L. R. Motowidlo, B. A. Zeitlin, M. S. Walker, and P. Haldar, *Appl. Phys. Lett.* **61**, 991 (1993).
- <sup>22</sup>I. Hlasnik *et al.*, *IEEE Trans. Appl. Supercond.* **3**, 1370 (1993).
- <sup>23</sup>K. Matsumoto, Y. Tanaka, K. Yamafuji, K. Funaki, M. Iwakuma, and T. Matsushita, *IEEE Trans. Appl. Supercond.* **3**, 1362 (1993).
- <sup>24</sup>R. W. Heussner, P. D. Jablonski, P. J. Lee, and D. C. Larbalestier, *IEEE Trans. Appl. Supercond.* **5**, 1705 (1995).
- <sup>25</sup>O. Miura, K. Matsumoto, Y. Tanaka, K. Yamafuji, N. Harada, M. Iwakuma, K. Funaki, and T. Matsushita, *Cryogenics* **32**, 315 (1992).
- <sup>26</sup>L. D. Cooley, Ph.D. thesis, University of Wisconsin-Madison, 1993.
- <sup>27</sup>C. Li and D. C. Larbalestier, *Cryogenics* **27**, 171 (1987).
- <sup>28</sup>L. D. Cooley, P. D. Jablonski, and D. C. Larbalestier (unpublished).
- <sup>29</sup>A. Gurevich and L. D. Cooley, *Phys. Rev. B* **50**, 13 563 (1994).
- <sup>30</sup>L. D. Cooley, A. Gurevich, and D. C. Larbalestier, in *Proceedings of the 7th International Workshop on Critical Currents in Superconductors*, edited by H. W. Weber (World Scientific, Singapore, 1994), p. 573.
- <sup>31</sup>P. J. Lee, D. C. Larbalestier, and P. D. Jablonski, *IEEE Trans. Appl. Supercond.* **5**, 1701 (1995).
- <sup>32</sup>W. A. Fietz and W. W. Webb, *Phys. Rev.* **178**, 657 (1969).
- <sup>33</sup>J. C. McKinnell, P. J. Lee, and D. C. Larbalestier, *IEEE Trans. Magn.* **25**, 1930 (1989); J. C. McKinnell, Ph.D. thesis, University of Wisconsin-Madison, 1990.
- <sup>34</sup>The lower critical field of the superconductor can be obtained from Ginzburg-Landau theory [see, e.g., C.-R. Hu, *Phys. Rev. B* **6**, 1756 (1972)] as  $H_{c1} = (\phi_0/4\pi\lambda^2)[\ln(\lambda/\xi) + \gamma_A]$  with  $\gamma_A = 0.50$ . On the other hand, a solution from London theory gives  $H_{c1} = (\phi_0/4\pi\lambda^2)[\ln(2\lambda/\xi) - C + \beta]$ , where  $\beta$  represents purely the core energy and  $C$  is the Euler constant. Thus  $\beta = 0.50 - \ln 2 + C = 0.38$  with  $\ln 2 - C \approx 0.12$ .
- <sup>35</sup>A. Barone and G. Paterno, *Physics and Applications of the Josephson Effect* (Wiley, New York, 1982).
- <sup>36</sup>A. Gurevich, *Phys. Rev. B* **46**, 3187 (1992).
- <sup>37</sup>A. Gurevich, *Phys. Rev. B* **48**, 12 857 (1993).
- <sup>38</sup>C. P. Bean and J. D. Livingston, *Phys. Rev. Lett.* **12**, 14 (1964).
- <sup>39</sup>G. Stejic, A. Gurevich, E. Kadyrov, D. Christen, R. Joynt, and D. C. Larbalestier, *Phys. Rev. B* **49**, 1274 (1994).
- <sup>40</sup>See Eq. (23) of Ref. 27.
- <sup>41</sup>P. G. deGennes, *Phys. Kondens. Mater.* **3**, 79 (1964).
- <sup>42</sup>K. Usadel, *Phys. Rev. Lett.* **25**, 507 (1970).
- <sup>43</sup>S. Takahashi and M. Tachiki, *Phys. Rev. B* **33**, 4620 (1986).
- <sup>44</sup>E. W. Collings, *A Sourcebook of Titanium Alloy Superconductivity* (Plenum, New York, 1983), pp. 53–74 and 213–242.
- <sup>45</sup>H. J. Muller, Ph.D. thesis, University of Wisconsin-Madison, 1991.
- <sup>46</sup>T. G. Berlincourt and R. R. Hake, *Phys. Rev.* **131**, 1 (1963).
- <sup>47</sup>A. C. Mota, P. Visani, and A. Pollini, *J. Low Temp. Phys.* **76**, 465 (1989).
- <sup>48</sup>D. S. Falk, *Phys. Rev.* **132**, 1576 (1963).
- <sup>49</sup>T. Akune, N. Sakamoto, O. Miura, Y. Tanaka, and K. Yamafuji, *J. Low Temp. Phys.* **94**, 219 (1994).
- <sup>50</sup>J. Aarts, K.-J. de Korver, and P. H. Kes, *Europhys. Lett.* **12**, 447 (1990).
- <sup>51</sup>T. Nojima, M. Kinoshita, S. Nakano, and Y. Kuwasawa, *Physica C* **205**, 387 (1993).
- <sup>52</sup>S. Takahashi and M. Tachiki, *Phys. Rev. B* **34**, 3162 (1986).
- <sup>53</sup>L. Dobrosavljević-Grujić and Z. Radović, *Supercond. Sci. Technol.* **6**, 537 (1993).
- <sup>54</sup>T. Y. Hsiang and D. K. Finnemore, *Phys. Rev. B* **22**, 154 (1980).
- <sup>55</sup>C. P. Bean, *Rev. Mod. Phys.* **36**, 31 (1964).
- <sup>56</sup>T. P. Orlando, E. J. McNiff, Jr., S. Foner, and M. R. Beasley, *Phys. Rev. B* **19**, 4545 (1979).
- <sup>57</sup>L. Burlachkov, M. Konczykowski, Y. Yeshurun, and F. Holzberg, *J. Appl. Phys.* **70**, 5759 (1991); L. Burlachkov, *Phys. Rev. B* **47**, 8056 (1993).
- <sup>58</sup>W. J. Carr, Jr. and G. R. Wagner, *J. Appl. Phys.* **60**, 342 (1986).
- <sup>59</sup>John R. Clem, in *Low Temperature Physics-LT 13*, edited by K. D. Timmerhaus, W. J. O'Sullivan, and E. F. Hammel (Plenum, New York, 1974), Vol. 3, p. 102.
- <sup>60</sup>L. D. Cooley and D. C. Larbalestier, in *Proceedings of the 8th U.S.-Japan Workshop on High-Field Superconducting Materials*, edited by K. Yamafuji and D. C. Larbalestier (Ministry of Education and Science and Technology Agency, Government of Japan, and U.S. Department of Energy, 1993), p. 92.
- <sup>61</sup>An error exists in Ref. 61, Eq. (2). The correct expression appears in Eq. (24).
- <sup>62</sup>D. P. Hampshire, A. F. Clark, and H. Jones, *J. Appl. Phys.* **66**, 3160 (1989).
- <sup>63</sup>D. P. Hampshire, K. E. Gray, and R. T. Kampwirth, *IEEE Trans. Appl. Supercond.* **3**, 1246 (1993).
- <sup>64</sup>H. Yamasaki, K. Endo, S. Kosaka, M. Umeda, S. Yoshida, and K. Kajimura, *Phys. Rev. Lett.* **70**, 3331 (1993); L. Civale, M. W. McElfresh, A. D. Marwick, F. Holtzberg, C. Feild, J. R. Thompson, and D. K. Christen, *Phys. Rev. B* **43**, 13 732 (1991).
- <sup>65</sup>P. D. Jablonski, Ph.D. thesis, University of Wisconsin-Madison, 1994.